Mechanical Properties of Bamboo-like Boron Nitride Nanotubes by *In Situ* TEM and MD Simulations: Strengthening Effect of Interlocked Joint Interfaces

Dai-Ming Tang,[†,‡,⊥] Cui-Lan Ren,[‡,⊥] Xianlong Wei,[†] Ming-Sheng Wang,[†,§] Chang Liu,[‡,*] Yoshio Bando,[†] and Dmitri Golberg[†,*]

[†]International Center for Materials Nanoarchitectonics (MANA), National Institute for Materials Science (NIMS), Namiki 1-1, Tsukuba, Ibaraki, 305-0044 Japan, and [‡]Shenyang National Laboratory for Materials Science, Institute of Metal Research, Chinese Academy of Sciences, 72 Wenhua Road, Shenyang 110016 China. [§]Present address: Laboratory for Nanophotonics and Electronics, Department of Materials Science and Engineering, Massachusetts Institute of Technology, Cambridge, Massachusetts 02139. [⊥]These authors contribute equally to this work.

ABSTRACT Understanding the influence of interfacial structures on the nanoarchitecture mechanical properties is of particular importance for its mechanical applications. Due to a small size of constituting nanostructural units and a consequently high volume ratio of such interfacial regions, this question becomes crucial for the overall mechanical performance. Boron nitride bamboo-like nanotubes, called hereafter boron nitride nanobamboos (BNNBs), are composed of short BN nanotubular segments with specific interfaces at the bamboo-shaped joints. In this work, the mechanical properties of such structures are investigated by using direct *in situ* transmission electron microscopy tensile tests and molecular dynamics simulations. The mechanical properties and deformation behaviors are correlated with the interfacial structure under atomic resolution, and a geometry strengthening effect is clearly demonstrated. Due to the interlocked joint interfacial structures and compressive interfacial stresses, the deformation mechanism is switched from an interplanar sliding mode to an in-plane tensile elongation mode. As a result of such a specific geometry strengthening effect, the BNNBs show high tensile fracture strength and Young's modulus up to 8.0 and 225 GPa, respectively.

KEYWORDS: boron nitride nanotube · interfacial geometry · mechanical properties · *in situ* TEM · MD simulation

One-dimensional nanomaterials are potential building blocks for high-performance nanoarchitectures because of their superior mechanical properties. Carbon nanotubes (CNTs) are extremely strong, having the fracture strength and Young's modulus up to 100 GPa and 1 TPa, respectively.[1−5] Boron nitride nanotubes (BNNTs) show fracture strength up to ~33 GPa and Young's modulus of 926 GPa.[6] In addition, many other one-dimensional materials, for example, metallic nanowires, such as Rh[7] and Au,[8] semiconducting nanowires, such as Si[9] and Ge,[10] and sulfide nanotubes, such as WS_2 and MoS_2,[11] show high strengths approaching the theoretically calculated limits. The excellent mechanical properties of the one-dimensional materials are ascribed to the absence or lack of defects, such as dislocations, grain boundaries, voids, and cracks.

In order to build a nanoarchitecture, it is important to have nanostructures connected and assembled through specific interfaces. In bulk polycrystalline materials, like metals, the yielding strength is mainly determined by the interactions between dislocations and grain boundaries rather than by strength of the single-crystalline grains. This correlation is well-established as the Hall−Petch relation.[12,13] In nanoarchitectures, due to a small size of the constituting nanoscale units, the volume ratio of the interfacial regions is much higher, and their influence on the nanoarchitecture mechanical properties becomes crucial. As an example, the strength of pure CNT yarns is determined by the shear strength between the nanotubes, rather than the tensile strength of the individual nanotubes,[14−16] and the mechanical performances of CNT- and BNNT-reinforced polymers are governed by the interfacial interactions between the nanotubes and a matrix.[17−20] Therefore, understanding the role of interface is a key for fabricating high-performance nanoarchitectures. Basically, the interfaces can be categorized into two types, that is, homogeneous and heterogeneous interfaces. The simplest interface would be a homogeneous interface linked by van der Waals interactions.[21−24] Interesting applications based on such interactions, such as gecko tapes and high-temperature rubbers, have been proposed.[23−25] Apparently, van der Waals interactions are not strong enough to be employed in

* Address correspondence to cliu@imr.ac.cn, golberg.dmitri@nims.go.jp.

Received for review June 20, 2011 and accepted August 8, 2011.

Published online August 08, 2011
10.1021/nn202283a

structural materials. Heterogeneous interfaces of CNTs have also been observed.[18,26−32] Wang *et al.* found that CNTs can form robust junctions with tungsten and cobalt, and these junctions possess tensile strengths as high as 4.7−14.8 and 1−5 GPa, respectively.[29,32] While heterogeneous interfaces have been demonstrated to be effective for a mechanical load transfer and electrical transport, the problems of interfacial chemical reactions, a lattice and/or thermal expansion coefficients mismatch still exist for the heterojunctions. Despite the extensive studies, a clear correlation between the interfacial structure and the mechanical properties of a nanoarchitecture has not been established as yet.

Boron nitride nanobamboos (BNNBs) are quasi-one-dimensional structures composed of short BN nanotubular segments.[33−36] Therefore, BNNBs are ideal model materials for investigating the influence of interfacial structure on the nanoarchitecture mechanical properties. In this study, the mechanical properties and deformation behavior of the BNNBs under tensile elongation are studied by *in situ* transmission electron microscopy (TEM) and molecular dynamics (MD) simulations. It is revealed that, by forming an interlocked joint interfacial structure, the deformation mechanism of the BNNBs is switched from an easy sliding to a resistant in-plane tensile elongation, which leads to the enhanced strength and Young's modulus up to 8.0 and 225 GPa, respectively.

RESULTS AND DISCUSSION

The experimental configuration for the *in situ* TEM tensile tests of the BNNBs is shown in Figure 1a. A BNNB was clamped with one end at the AFM cantilever and the other end at the W tip by an electron-beam-induced deposition (EBID) technique. The BNNBs were stretched by retracting the W tip until they were ruptured (Supporting Information, movie S1). Figure 1b,c shows TEM images of a BNNB before and after the tensile test. The inner and outer diameters and length of the BNNBs are 23.5, 27.5, and 330 nm, respectively. The bamboo units are about 110 nm in length with a "yard-glass" shape, with one end open and the other one closed. A HRTEM image of the bamboo joint is shown in Figure 1d. The BN (002) planes with an interplane distance of 0.33 nm are clearly resolved, indicating the high tube crystallinity. The lattices of the neighboring bamboo units are discontinuous at the bamboo joints (Figure S1). The BN (002) planes are overlapped from the end section (A−A) to (B−B) with the largest diameter, and to the (C−C) section with a decreased diameter. Therefore, the interface at the joint is inclined to form an interlocked structure rather than being straight and parallel to the tube axis. Figure 1e demonstrates the fractured end after the BNNB has been broken under tension. The fractured end was expanded during the tensile

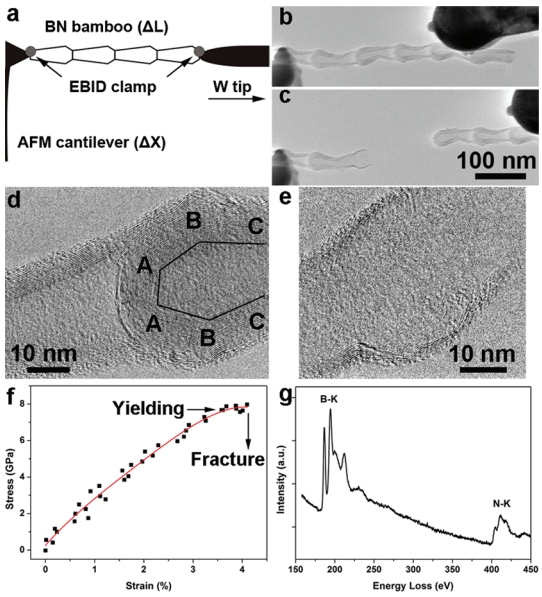

Figure 1. (a) Schematic showing the tensile elongation run on a BNNB. EBID is used for clamping both ends of the BNNB. The W tip is driven by a piezo tube. The cantilever displacement (Δx) and elongation of the BNNB (ΔL) are *in situ* video recorded. (b,c) TEM images of a BNNB before (b) and after (c) a tensile test. (d) HRTEM image of the bamboo joint. It is pear-shaped, with the largest diameter at the (B−B) section. The interface is made from (A−A), (B−B), and (C−C) sections, for the latter the diameter shrinks to form an interlocked structure. (e) HRTEM image of the fractured BNNB. (f) Typical experimental stress−strain plot (black rectangles), along with a fitted curve shown in red. The BNNB deforms elastically until yielding starts to take place at ~3.5%, after which the stress−strain plot deviates from a linear relationship, and finally fracture occurs at a total strain of ~4.1%. (g) EEL spectrum of the BNNB after fracture. Boron and nitrogen K-edges are clearly identified, and no carbon K-edge could be detected.

elongation process, and the summing of four inner angles gave the values of 513 and 544° for the initial and final states, respectively. Figure 1f shows a typical stress−strain curve. The curve is linearly shaped until the strain reaches about 3.5%. At the final stage, the curve deviates from the linear relationship, implying yielding and a plastic deformation, and the BNNB ruptures at the maximum strain of ~4.1%. By measuring the displacement of the AFM cantilever, the applied force was obtained and the maximum force drop was calculated to be ~1003 nN. Correspondingly, the fracture strength was calculated using the following formula: $\sigma = (k\Delta x/\cos\alpha)/S$, where k = 6.9 N/m is the spring constant of the AFM cantilever, Δx is the measured displacement of the AFM cantilever, α is the angle between the BNNB and the movement direction of the AFM cantilever, and $S = \pi(d_o^2 - d_i^2)/4$ is the cross-section area of the fractured end, where d_o and d_i are the outer and inner diameters, respectively. The strain was obtained by measuring the elongation of the BNNB using video snap shots. The fracture strength and Young' modulus were calculated to be ~8.0 and ~225 GPa, respectively.

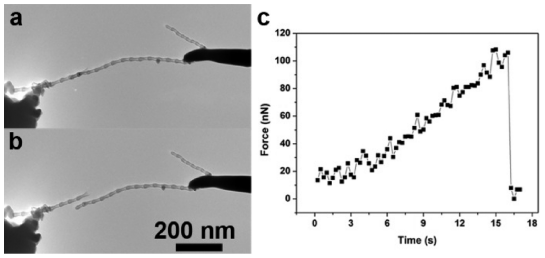

Figure 2. (a,b) TEM images of the BNNBs joined through van der Waals interactions before (a) and after (b) a tensile test. (c) Time−force curve of the test. A force drop around 96 nN was measured.

The measured strength of the BNNBs is about 5 times that of high strength steel and is comparable with WS_2 nanotubes,[11] Au[8] and Si[9] nanowires, and as strong as the CNT−metal heterojunctions.[29,32] Due to the discontinuity of the lattice, it is natural that the mechanical properties of BNNBs are inferior to those of individual standard BNNTs[6] and CNTs.[1−5] However, considering that the BNNBs are composed of BNNT units with discontinuous lattices at the bamboo joints, where only van der Waals interactions, rather than covalent bonding, should be taken into account, the present BNNBs are surprisingly strong. To get additional insight with regard to this phenomenon, the van der Waals interactions between BNNBs were studied, as shown in Figure 2. After the fracture of the BNNB, the fractured ends were navigated to approach each other. When they became close enough, a side to side contact was formed due to the van der Waals attraction. Then a tensile force was applied to measure the attraction force. The measured force drop was about 96 nN, about 10 times smaller than that measured for BNNBs in the preceding experiment. The overlapping part is ~87 nm in length, which is more than twice of the length of a typical bamboo joint. Therefore, the strength of BNNBs is much higher than that expected from sole van der Waals interactions. Additionally, *in situ* TEM observations of the deformation under compression and bending showed that the BNNBs are highly flexible and tough (Figures S2 and S3 in the Supporting Information). As shown in the HRTEM images in Figure 1d,e, no carbon deposit was found at the BNNB surface. In addition, an electron energy loss spectrum (EELS) taken from the BNNB after fracture (Figure 1g) identified only boron and nitrogen K-edges, and no carbon signal was detected. *In situ* electrical measurements on a clamped BNNB gave an $I-V$ curve presented in Figure S4. Within a bias range of ±5 V, only a noise current of ~1 nA could be measured, confirming that the insulating BNNBs are free of carbon contamination. Therefore, the strengthening of the BNNB is not caused by the change of chemical composition or bonding. As depicted in Figure 1d,e, the interfaces between the bamboo units are special; that is, an interlocked structure with a narrowing closure is

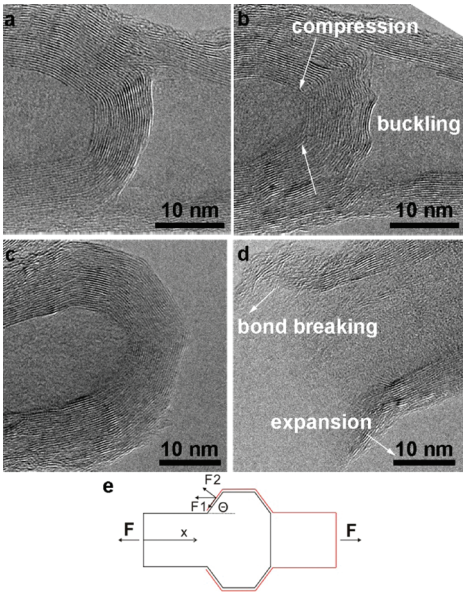

Figure 3. (a,b) HRTEM images of a BNNB during the tensile test. The buckling ripples due to compressive interfacial stresses are marked by arrows. (c,d) HRTEM images of the fractured BNNB. The traces of bond breaking and expansion are indicated by arrows. (e) Schematic picture of a BN bamboo joint. The applied tensile stress F induces interfacial stresses F_1 and F_2, parallel and perpendicular to the interface, respectively; θ is the angle between the interface and the tensile elongation direction.

formed. Mechanical properties are strongly dependent on the structures. Standard BN nanotubes consist of concentric rolled layers stacked up *via* van der Waals forces. Each layer is a continuous BN rolled (002) plane, in which strong covalent bonding dominates. Wei *et al.* reported the tensile tests of BN nanotubes. Similar to CNTs, the BN nanotubes fracture in a brittle manner and show high tensile strength up to several tens of GPa and high Young's modulus up to around 1 TPa.[6] After the breakage of the outer layers, the inner layers can be pulled out by sliding under a very low stress.[43] BNNBs are composed of short BN nanotubes. Most importantly, BNNBs are quite different from BN nanotubes; that is, there are no continuous BN planes extending through the neighboring bamboo segments (Figure S1). BNNBs are also different from the BN nanotubes with the broken outer layers; for example, the bamboo joint forms an interlocked structure with non-uniform diameters, and the inner and outer parts cannot slide freely. Therefore, the strengthening of the BNNBs should be ascribed to this special interface geometry.

It was found that the interfacial geometry has important influence on the deformation mechanism and fracture behaviors by further *in situ* observation of the structural evolution during and after the tensile elongation, as shown in Figure 3. Under a tensile stress, the bamboo joint started to show rippling of the BN (002) planes as a result of buckling, which can be ascribed to a compressive stress at the interface (Figure 3a,b), which could restrict the interlayer sliding and enhance

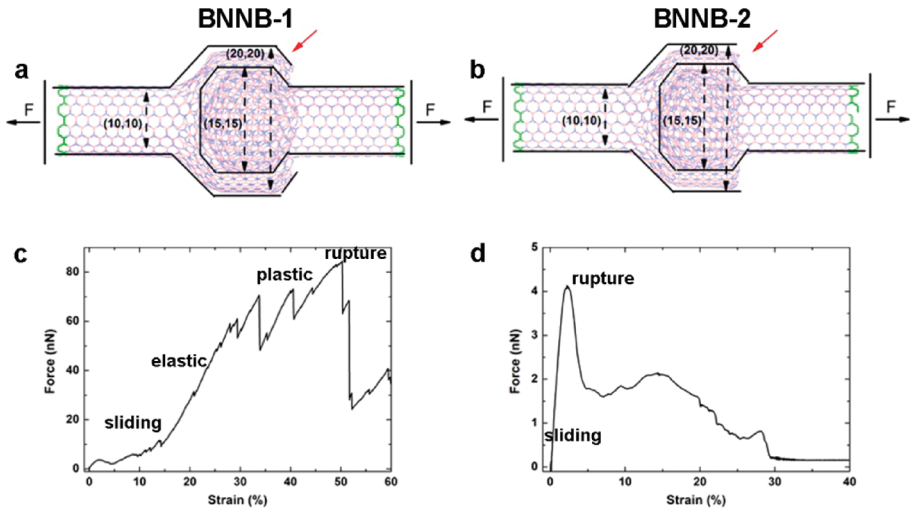

Figure 4. Schematic simulation setups of the tensile elongation for BNNB-1 (a) with a specific interlocked interfacial structure and BNNB-2 (b) with a nonconstrained interface. The difference of the joint geometries is marked by the red arrows. The green parts of the two ends are fixed during the structural relaxation. The pink and blue spheres denote B and N atoms, respectively. Computed force−strain curves for BNNB-1 (c) and BNNB-2 (d), with the maximum forces around 84.5 and 4.1 nN, respectively.

the mechanical properties. Figure 3c,d shows HRTEM images of the fractured portions. The interfacial compressive stress was released after the rupture, and the buckled inner part of the joint recovered to its original shape (Figure 3c). Similar to Figure 1e, the open end of the joint has been expanded, due to the interfacial compressive stress. More importantly, a trace of tearing and resultant bond breaking is observed (Figure 3d). It is possible that the breakage of the BNNB started from cracking of the outer part of the bamboo joint, corresponding to the observed yielding. When the crack became long enough, the geometrical constraint failed and the BNNB rapidly fractured (Figure 1f).

To reveal the nature of the interfacial interactions and the specific mechanism of the strengthening effects, a simplified model was built for the mechanical analysis of the BN bamboo structure (Figure 3e). Under a tensile elongation, the applied tensile stress F induces the interfacial stresses F_1 and F_2, parallel and normal to the interface, respectively. The interfacial stresses are calculated as follows: $F_1 = F\cos(\theta)$, $F_2 = F\sin(\theta)$, where θ is the angle of the inclined interface to the nanotube axis. When the strain is small and the deformation is elastic, the corresponding strains are calculated as $x_1 = (F_1\cos(\theta))/E_1$, $x_2 = (F_2\sin(\theta))/E_2$, where x_1 and x_2 are the strains in horizontal direction due to the corresponding stress, and E_1 and E_2 are the corresponding elastic moduli of h-BN in the parallel and perpendicular directions, respectively. Therefore, the Young's modulus of the BNNB joint portion is calculated as $E_j = ((\cos^2\theta/E_1) + (\sin^2\theta/E_2))^{-1}$, and the Young's modulus of the whole BNNB is calculated using the following formula: $E = (k/E_t + (1-k)/E_j)^{-1}$, where E_t is the Young's modulus of h-BN in tension, and k and $1-k$ are the percentages of the nanotube body and joint portions, respectively. The deformation of the BNNB joint is first presumed as the combination of interplanar compression and shear deformation, therefore, $E_1 = E_s \sim 3.0$ GPa and $E_2 = E_c \sim 34.6$ GPa are used for the calculations, where E_s and E_c are the elastic moduli of h-BN in interplanar shear and compression, respectively.[37−39] By taking the values for $\theta = 45°$, $k = 0.7$, the Young's modulus of the BNNB is calculated to be 18.1 GPa. However, the measured Young's modulus of the BNNBs is 225 GPa, which is about 12 times that of the calculated value from such simplified analysis. Therefore, the utilized presumption for the deformation mode is not appropriate, and a new deformation mechanism should be considered. It is noticeable that the sliding deformation is actually constrained by the geometry when the two layers of the joint get into contact. For further deformation, its mode has to be switched from the interplanar sliding to in-plane tensile elongation, of which the elastic modulus is up to 884−1220 GPa.[6,37−40] Accordingly, the tensile Young's modulus of h-BN was attempted as E_1 for the calculations, and the Young's modulus of the BNNB was then calculated to be 188.8−198.8 GPa, which is close to our *in situ* TEM experimental value. The difference of the estimated value and the measurement result may be caused by the diverse cross section of the BN nanotubes.[6,41,42] Therefore, the mechanism of the strengthening effect is attributed to the constraint originated from the interlocked interfacial geometry and the resultant deformation conversion from an easy interplanar sliding mode to a resistant in-plane tensile elongation mode.

Then MD simulations were performed to compare the strength and deformation behaviors of BNNBs with two types of interfacial geometries and to better understand the interfacial geometry strengthening effect. The schematic simulation setups are shown in Figure 4a,b. The BNNBs are composed of two single-walled BN nanotubes with varying diameters and the

(*m*,*n*) indexes as marked in the schemes. BN-nanocones with a disclination angle of 60° were used to connect the BN nanotubes with different non-six-membered rings. All of the B and N atoms maintained sp^2 configurations in order to achieve a maximized stability. These models were relaxed using conjugate gradient method. As indicated by the arrows, the difference of the two initial models is that the model in Figure 4a (BNNB-1) has a diameter decreasing closure to form an interlocked structure, while the model in Figure 4b (BNNB-2) is open with parallel and horizontal basal planes. Figure 4c,d shows the computed force−strain curves of the BNNBs. For BNNB-1, the force first increased gradually, indicating an easy sliding stage, until the tensile force and strain reached 11.0 nN and 14.9%, respectively. By using the cross-section area of the (20,20) nanotube, the modulus of the easy sliding stage was calculated to be 51.0 GPa. Then the gradient increased, indicating that the two parts of the bamboo joint established a tight contact. Corresponding modulus of the tight contact stage was calculated to be 252.6 GPa. After that, abrupt force drops were observed, indicating yielding and plastic deformation, which is consistent with the *in situ* TEM measurements and observations. Finally, the BNNB was ruptured at the maximum force of around 84.5 nN. For BNNB-2, it was broken in a brittle manner with an elastic process followed by a major force drop at the maximum force of 4.1 nN, which is consistent with the van der Waals force measurements on individual CNTs.[43] The strength of BNNB-1 with the interlocked joint structure is more than 20 times higher than that of BNNB-2 that is only joined by pure van der Waals interactions in accord with our *in situ* TEM data.

Snapshots of the MD simulation are demonstrated in Figure 5 to display the deformation and fracture processes of the BNNBs. During the tensile elongation, for BNNB-1 (movie S2 in the Supporting Information), the two layers first slip (a), marking the first easy sliding stage. Then an expansion of the outer layer due to the compressive interfacial stress takes place (b), corresponding to the tight contact stage. With an increase of interfacial stress, buckling of the BN plane becomes apparent (c), corresponding to plastic deformation. Finally, BNNB-1 is ruptured along with breaking bonds (d), resulting in final fracture. The observed deformation processes fully support the regarded geometry strengthening mechanism. At the initial stage, the easy interplanar shear and sliding deformation mode dominates. Then, the deformation mode is switched to in-plane tensile elongation due to the geometrical constraint.

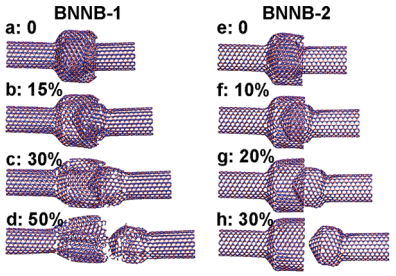

Figure 5. Snapshots of MD simulation for the tensile elongation of BNNB-1 (a−d) and BNNB-2 (e−h) with the tensile strain marked. During the elongation, sliding (a), tight contacting and in-plane elongation (b), buckling (c), and bond breaking (d) are observed for BNNB-1 at different stages, while BNNB-2 is broken by sole sliding (e−h).

Because of a short distance between the inner and outer portions of the BNNB joint, the first deformation stage has not been observed during the *in situ* TEM tensile tests. For BNNB-2 (movie S3), only easy sliding has been noticed until the two layers become fully separated. The dramatic difference of the deformation and fracture behaviors and over 20-fold enhancement of strength of BNNB-1 compared with BNNB-2 are associated with the peculiar interfacial structure, that is, the interlocked structure experiencing compressive interfacial stresses and resultant conversion of deformation mechanisms.

In conclusion, the mechanical properties of BNNBs under tensile elongation are studied by *in situ* TEM and MD simulations in order to get insights into the influence of interfacial geometry on the mechanical properties of nanoarchitectures. While possessing homogeneous interfaces with only van der Waals forces acting between bamboo-like joints, the BNNBs show surprisingly high tensile fracture strength and Young's modulus up to 8.0 and 225 GPa, respectively. The geometry strengthening effect is ascribed to an interlocked interface experiencing compressive interfacial stresses. Because of the interfacial interactions, the deformation mechanism is switched from interplanar sliding between the inner and outer walls to in-plane tensile elongation of the outer layers. Accordingly, the BNNB fractures *via* cracking of the outer layers, subsequent yielding, and final complete separation of the bamboo segments. Molecular dynamics simulations of the tensile elongation of BNNBs agree well with the proposed geometry strengthening effect. A BNNB with the interlocked interface is found to be 20 times stronger than the BNNB with the nonconstrained interface. Our work demonstrates that the interfacial geometry is crucially important to enhance the mechanical performances of a nanoarchitecture.

METHODS

Synthesis of Boron Nitride Nanobamboos (BNNBs). The BNNBs were produced by a floating catalyst chemical vapor deposition method at 1300 °C by using ferrocene as a floating catalyst precursor, boron and boron oxide as a boron source, and ammonia as a nitrogen source.[35,36]

***In Situ* TEM Mechanical Tests.** A two-step approach was used during the mechanical tests.[5,6,29,44] First, a suitable BNNB was selected and transferred to a STM tip using a TEM-STM holder (Nanofactory Instruments AB). Second, the mechanical tests were carried out by using a TEM-AFM (also Nanofactory Instruments AB) holder. A sharp tungsten tip prepared by electrochemical etching was used as the STM tip, on which a tiny wax droplet was placed for electron-beam-induced deposition (EBID) of carbon clamps for tensile testing.[6,45] After the Au wire with a sample and W tip with wax were mounted into the TEM-STM holder, the holder was inserted into the TEM (JEOL-3100 FEF with an Omega filter applicable for the electron energy loss spectroscopy (EELS) and a CCD camera for imaging and real-time video recording). The W tip was driven by a piezo tube to be precisely aligned with the selected nanotube sample. Then, the intimate physical contact was made. The electron beam was focused at the boundary of the sample and tip for a few minutes to induce EBID carbon deposition for reliable clamping of BNNBs. By choosing the suitable electron beam conditions, the clamp was highly localized close to the sample end and the surface of the BNNB was free of carbon deposition. Then the selected BNNB was cut for further mechanical tests by a focused convergent electron beam or by a rapid retraction of the W tip. The W tip with a BNNB clamped was transferred to the TEM-AFM holder. A clamp between the BNNB and AFM cantilever was analogously formed by EBID. After that, the tip retraction was performed, while the sample displacement and its structural evolution were recorded by video and TEM imaging.

Before the tensile tests, the parameters of the AFM force sensors were calibrated by pushing the tungsten tip against the AFM cantilever. The nominal spring constant of the AFM cantilever used in this work was 6.9 N/m. The noise level of the AFM sensor was ~5−8 nN. The force drop measured for the BNNB was ~1003 nN, therefore giving an error for the fracture stress calculations of ~0.5 to 0.8%. In order to reduce the error of elongation measurements and related strain calculations, the sample and tungsten tip were adjusted to be at the same height of the AFM cantilever using the wobbler function of the microscope. Video snaps were used for the measurements of elongations, of which one pixel was ~0.5 nm. Compared with the total elongation of approximately 14.9 nm, the error of the fracture strain calculations was determined to be ~3.4%.

Molecular Dynamics (MD) Simulations. The mechanical properties of BNNBs were studied by MD simulations with empirical potentials. The interaction between boron and nitrogen atoms was modeled by Tersoff-like potential.[46] The parameters for B and N were taken from ref 47. The van der Waals interactions were modeled by Lennard-Jones (LJ) potential. The LJ parameters used in this paper were as follows: ε_{boron} = 0.004116 eV, σ_{boron} = 3.453 Å, $\varepsilon_{nitrogen}$ = 0.006281 eV, and $\sigma_{nitrogen}$ = 3.365 Å.[48] The boron−nitrogen parameters were obtained using Lorentz−Berthelot mixing rules, $\varepsilon_{ab} = (\varepsilon_a\varepsilon_b)^{1/2}$ and $\sigma_{ab} = (\sigma_a + \sigma_b)/2$. The classical equations of motion were integrated by velocity Verlet algorithm with a fixed time step of 0.5 fs for the simulations.[49,50] For the tensile elongation simulations, the stretching rate was 0.04 Å/ps. During the stretching process, a strain increment of 0.01 Å was applied to the two ends of the model, and two layers of atoms at the two ends were fixed during the structure optimization. The environmental temperature of the simulation was maintained at 0.5 K by using the Berendsen thermostat to eliminate the effect of thermal fluctuations.

Acknowledgment. The work was supported by the International Center for Materials Nanoarchitectonics (MANA) of the National Institute for Materials Science (NIMS), Tsukuba, Japan, and MOST (Grant 2011CB932601), and NSFC (Grants 50921004 and 50872137), China. The authors thank M. Mitome and I. Yamada of MANA-NIMS for technical support.

Supporting Information Available: In situ TEM video of the tensile test of a BNNB; MD simulation videos of the tensile elongation of BNNB-1 and BNNB-2; HRTEM image of a whole bamboo joint; *in situ* TEM observations of the BNNBs under compression and bending. *I*−*V* curve of a clamped BNNB. This material is available free of charge *via* the Internet at http://pubs.acs.org.

REFERENCES AND NOTES

1. Treacy, M. M. J.; Ebbesen, T. W.; Gibson, J. M. Exceptionally High Young's Modulus Observed for Individual Carbon Nanotubes. *Nature* **1996**, *381*, 678–680.
2. Yu, M. F.; Files, B. S.; Arepalli, S.; Ruoff, R. S. Tensile Loading of Ropes of Single Wall Carbon Nanotubes and Their Mechanical Properties. *Phys. Rev. Lett.* **2000**, *84*, 5552.
3. Yu, M. F.; Lourie, O.; Dyer, M. J.; Moloni, K.; Kelly, T. F.; Ruoff, R. S. Strength and Breaking Mechanism of Multiwalled Carbon Nanotubes under Tensile Load. *Science* **2000**, *287*, 637–640.
4. Peng, B.; Locascio, M.; Zapol, P.; Li, S.; Mielke, S. L.; Schatz, G. C.; Espinosa, H. D. Measurements of Near-Ultimate Strength for Multiwalled Carbon Nanotubes and Irradiation-Induced Crosslinking Improvements. *Nat. Nanotechnol.* **2008**, *3*, 626–631.
5. Wang, M. S.; Golberg, D.; Bando, Y. Tensile Tests on Individual Single-Walled Carbon Nanotubes: Linking Nanotube Strength with Its Defects. *Adv. Mater.* **2010**, *22*, 4071–4075.
6. Wei, X.; Wang, M. S.; Bando, Y.; Golberg, D. Tensile Tests on Individual Multi-walled Boron Nitride Nanotubes. *Adv. Mater.* **2010**, *22*, 4895–4899.
7. Philippe, L.; Wang, Z.; Peyrot, I.; Hassel, A. W.; Michler, J. Nanomechanics of Rhenium Wires: Elastic Modulus, Yield Strength and Strain Hardening. *Acta Mater.* **2009**, *57*, 4032–4035.
8. Wu, B.; Heidelberg, A.; Boland, J. J. Mechanical Properties of Ultrahigh-Strength Gold Nanowires. *Nat. Mater.* **2005**, *4*, 525–529.
9. Zhu, Y.; Xu, F.; Qin, Q.; Fung, W. Y.; Lu, W. Mechanical Properties of Vapor−Liquid−Solid Synthesized Silicon Nanowires. *Nano Lett.* **2009**, *9*, 3934–3939.
10. Smith, D. A.; Holmberg, V. C.; Korgel, B. A. Flexible Germanium Nanowires: Ideal Strength, Room Temperature Plasticity, and Bendable Semiconductor Fabric. *ACS Nano* **2010**, *4*, 2356–2362.
11. Kaplan-Ashiri, I.; Cohen, S. R.; Gartsman, K.; Ivanovskaya, V.; Heine, T.; Seifert, G.; Wiesel, I.; Wagner, H. D.; Tenne, R. On the Mechanical Behavior of WS_2 Nanotubes under Axial Tension and Compression. *Proc. Natl. Acad. Sci. U.S.A.* **2006**, *103*, 523–528.
12. Hall, E. O. The Deformation and Ageing of Mild Steel: III Discussion of Results. *Proc. Phys. Soc. London, Ser. B* **1951**, *64*, 747.
13. Petch, N. J. The Cleavage of Polycrystals. *J. Iron Steel Inst.* **1953**, *174*, 25–28.
14. Zhu, H. W.; Xu, C. L.; Wu, D. H.; Wei, B. Q.; Vajtai, R.; Ajayan, P. M. Direct Synthesis of Long Single-Walled Carbon Nanotube Strands. *Science* **2002**, *296*, 884–886.
15. Zhang, M.; Atkinson, K. R.; Baughman, R. H. Multifunctional Carbon Nanotube Yarns by Downsizing an Ancient Technology. *Science* **2004**, *306*, 1358–1361.
16. Vilatela, J. J.; Elliott, J. A.; Windle, A. H. A Model for the Strength of Yarn-like Carbon Nanotube Fibers. *ACS Nano* **2011**, *5*, 1921–1927.
17. Mamedov, A. A.; Kotov, N. A.; Prato, M.; Guldi, D. M.; Wicksted, J. P.; Hirsch, A. Molecular Design of Strong Single-Wall Carbon Nanotube/Polyelectrolyte Multilayer Composites. *Nat. Mater.* **2002**, *1*, 190–194.
18. Coleman, J. N.; Cadek, M.; Blake, R.; Nicolosi, V.; Ryan, K. P.; Belton, C.; Fonseca, A.; Nagy, J. B.; Gun'ko, Y. K.; Blau, W. J. High Performance Nanotube-Reinforced Plastics: Understanding the Mechanism of Strength Increase. *Adv. Funct. Mater.* **2004**, *14*, 791–798.
19. Zhi, C. Y.; Bando, Y.; Tang, C. C.; Honda, S.; Kuwahara, H.; Golberg, D. Boron Nitride Nanotubes/Polystyrene Composites. *J. Mater. Res.* **2006**, *21*, 2794–2800.
20. Liu, K.; Sun, Y.; Lin, X.; Zhou, R.; Wang, J.; Fan, S.; Jiang, K. Scratch-Resistant, Highly Conductive, and High-Strength Carbon Nanotube-Based Composite Yarns. *ACS Nano* **2010**, *4*, 5827–5834.
21. Thomsen, C.; Reich, S.; Goñi, A. R.; Jantoljak, H.; Rafailov, P. M.; Loa, I.; Syassen, K.; Journet, C.; Bernier, P. Intermolecular

Interaction in Carbon Nanotube Ropes. *Phys. Status Solidi B* **1999**, *215*, 435–441.
22. Sun, C. H.; Yin, L. C.; Li, F.; Lu, G. Q.; Cheng, H. M. van der Waals Interactions between Two Parallel Infinitely Long Single-Walled Nanotubes. *Chem. Phys. Lett.* **2005**, *403*, 343–346.
23. Ge, L.; Sethi, S.; Ci, L.; Ajayan, P. M.; Dhinojwala, A. Carbon Nanotube-Based Synthetic Gecko Tapes. *Proc. Natl. Acad. Sci. U.S.A.* **2007**, *104*, 10792–10795.
24. Xu, M.; Futaba, D. N.; Yamada, T.; Yumura, M.; Hata, K. Carbon Nanotubes with Temperature-Invariant Viscoelasticity from −196° to 1000°C. *Science* **2010**, *330*, 1364–1368.
25. Qu, L.; Dai, L.; Stone, M.; Xia, Z.; Wang, Z. L. Carbon Nanotube Arrays with Strong Shear Binding-On and Easy Normal Lifting-Off. *Science* **2008**, *322*, 238–242.
26. Qian, D.; Dickey, E. C.; Andrews, R.; Rantell, T. Load Transfer and Deformation Mechanisms in Carbon Nanotube–Polystyrene Composites. *Appl. Phys. Lett.* **2000**, *76*, 2868–2870.
27. Kis, A.; Csányi, G.; Salvetat, J. P.; Lee, T. N.; Couteau, E.; Kulik, A. J.; Benoit, W.; Brugger, J.; Forró, L. Reinforcement of Single-Walled Carbon Nanotube Bundles by Intertube Bridging. *Nat. Mater.* **2004**, *3*, 153–157.
28. Rodríguez Manzo, J. A.; Banhart, F.; Terrones, M.; Terrones, H.; Grobert, N.; Ajayan, P. M.; Sumpter, B. G.; Meunier, V.; Wang, M.; Bando, Y.; *et al.* Heterojunctions between Metals and Carbon Nanotubes as Ultimate Nanocontacts. *Proc. Natl. Acad. Sci. U.S.A.* **2009**, *106*, 4591–4595.
29. Wang, M. S.; Bando, Y.; Rodríguez Manzo, J. A.; Banhart, F.; Golberg, D. Cobalt Nanoparticle-Assisted Engineering of Multiwall Carbon Nanotubes. *ACS Nano* **2009**, *3*, 2632–2638.
30. Tang, D. M.; Yin, L. C.; Li, F.; Liu, C.; Yu, W. J.; Hou, P. X.; Wu, B.; Lee, Y. H.; Ma, X. L.; Cheng, H. M. Carbon Nanotube-Clamped Metal Atomic Chain. *Proc. Natl. Acad. Sci. U.S.A.* **2010**, *107*, 9055–9059.
31. Wang, M. S.; Golberg, D.; Bando, Y. Interface Dynamic Behavior between a Carbon Nanotube and Metal Electrode. *Adv. Mater.* **2010**, *22*, 93–98.
32. Wang, M. S.; Golberg, D.; Bando, Y. Superstrong Low-Resistant Carbon Nanotube–Carbide–Metal Nanocontacts. *Adv. Mater.* **2010**, *22*, 5350–5355.
33. Chen, Y.; Chadderton, L. T.; Gerald, J. F.; Williams, J. S. A Solid-State Process for Formation of Boron Nitride Nanotubes. *Appl. Phys. Lett.* **1999**, *74*, 2960–2962.
34. Chadderton, L. T.; Chen, Y. A Model for the Growth of Bamboo and Skeletal Nanotubes: Catalytic Capillarity. *J. Cryst. Growth* **2002**, *240*, 164–169.
35. Chen, Z. G.; Zou, J.; Li, F.; Liu, G.; Tang, D. M.; Li, D.; Liu, C.; Ma, X. L.; Cheng, H. M.; Lu, G. Q.; *et al.* Growth of Magnetic Yard-Glass Shaped Boron Nitride Nanotubes with Periodic Iron Nanoparticles. *Adv. Funct. Mater.* **2007**, *17*, 3371–3376.
36. Tang, D. M.; Liu, C.; Cheng, H. M. Controlled Synthesis of Quasi-One-Dimensional Boron Nitride Nanostructures. *J. Mater. Res.* **2007**, *22*, 2809–2816.
37. Edgar, J. H. *Properties of Group III Nitrides*; Institution of Engineering and Technology, 1994.
38. Ooi, N.; Rajan, V.; Gottlieb, J.; Catherine, Y.; Adams, J. B. Structural Properties of Hexagonal Boron Nitride. *Modell. Simul. Mater. Sci. Eng.* **2006**, *14*, 515.
39. Hamdi, I.; Meskini, N. *Ab Initio* Study of the Structural, Elastic, Vibrational and Thermodynamic Properties of the Hexagonal Boron Nitride: Performance of LDA and GGA. *Physica B* **2010**, *405*, 2785–2794.
40. Chopra, N. G.; Zettl, A. Measurement of the Elastic Modulus of a Multi-wall Boron Nitride Nanotube. *Solid State Commun.* **1998**, *105*, 297–300.
41. Celik-Aktas, A.; Zuo, J. M.; Stubbins, J. F.; Tang, C. C.; Bando, Y. Double-Helix Structure in Multiwall Boron Nitride Nanotubes. *Acta Crystallogr. A* **2005**, *61*, 533–541.
42. Golberg, D.; Mitome, M.; Bando, Y.; Tang, C. C.; Zhi, C. Y. Multi-walled Boron Nitride Nanotubes Composed of Diverse Cross-Section and Helix Type Shells. *Appl. Phys. A* **2007**, *88*, 347–352.
43. Akita, S.; Nakayama, Y. Interlayer Sliding Force of Individual Multiwall Carbon Nanotubes. *Jpn. J. Appl. Phys.* **2003**, *42*, 4830–4833.
44. Rodríguez Manzo, J. A.; Wang, M. S.; Banhart, F.; Bando, Y.; Golberg, D. Multibranched Junctions of Carbon Nanotubes *via* Cobalt Particles. *Adv. Mater.* **2009**, *21*, 4477.
45. Ding, W.; Dikin, D. A.; Chen, X.; Piner, R. D.; Ruoff, R. S.; Zussman, E.; Wang, X.; Li, X. Mechanics of Hydrogenated Amorphous Carbon Deposits from Electron-Beam-Induced Deposition of a Paraffin Precursor. *J. Appl. Phys.* **2005**, *98*, 014905–014907.
46. Tersoff, J. New Empirical Approach for the Structure and Energy of Covalent Systems. *Phys. Rev. B* **1988**, *37*, 6991.
47. Albe, K.; Möller, W.; Heinig, K.-H. Computer Simulation and Boron Nitride. *Radiat. Eff. Defects Solids* **1997**, *141*, 85–97.
48. Lee, J. H. A Study on a Boron–Nitride Nanotube as a Gigahertz Oscillator. *J. Korean Phys. Soc.* **2006**, *49*, 172–176.
49. Verlet, L. Computer "Experiments" on Classical Fluids. I. Thermodynamical Properties of Lennard-Jones Molecules. *Phys. Rev.* **1967**, *159*, 98.
50. Verlet, L. Computer "Experiments" on Classical Fluids. II. Equilibrium Correlation Functions. *Phys. Rev.* **1968**, *165*, 201.